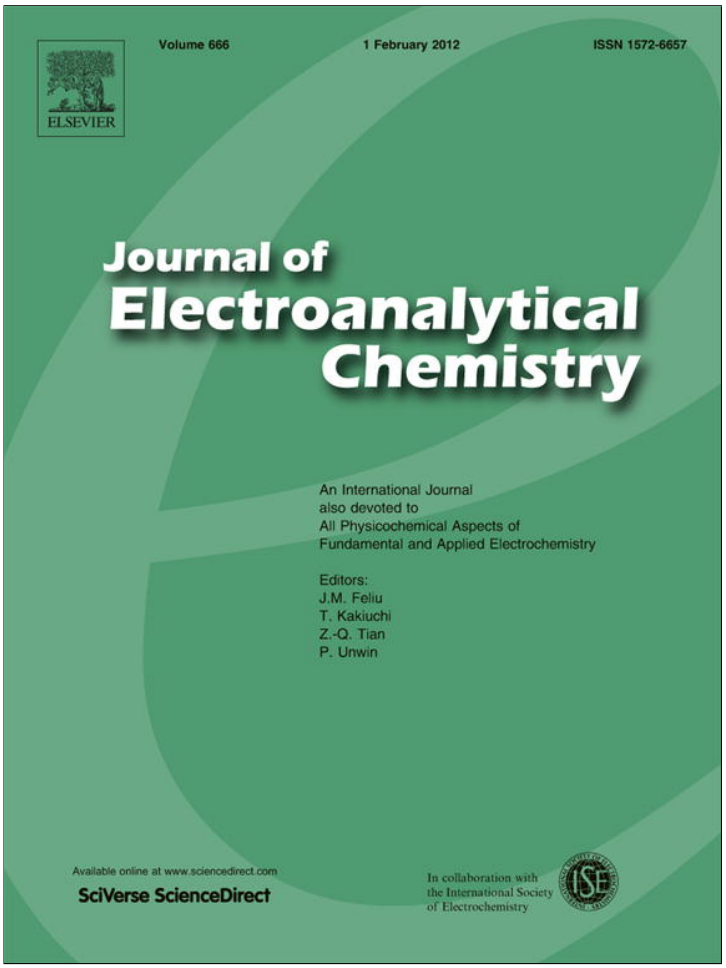

Journal of Electroanalytical Chemistry 666 (2012) 42–51

Contents lists available at SciVerse ScienceDirect

Journal of Electroanalytical Chemistry

journal homepage: www.elsevier.com/locate/jelechem

Ion transfer across liquid|liquid interface under forced hydrodynamic conditions. I: Digital simulations

Juan Manuel Ovejero, Ricardo Ariel Fernández, Sergio Alberto Dassie *

Instituto de Investigaciones en Fisicoquímica de Córdoba (INFIQC), Departamento de Fisicoquímica, Facultad de Ciencias Químicas, Universidad Nacional de Córdoba, Ciudad Universitaria, Córdoba X5000HUA, Argentina

ARTICLE INFO

Article history:
Received 27 September 2011
Received in revised form 24 November 2011
Accepted 25 November 2011
Available online 3 December 2011

Keywords:
Digital simulation
Finite difference
Facilitated ion transfer
Liquid|liquid interface
Forced hydrodynamic conditions

ABSTRACT

In this paper, we present the general equations for a model that describes ion transfer reactions across the oil|water interface assisted by a ligand, under forced hydrodynamic conditions. Our analysis is mainly focused on the effect of mechanical stirring of the aqueous or organic phase during the potential sweep, and its influence on the limiting diffusion currents. The model was solved numerically using explicit finite difference; the results of digital simulations are obtained for simple and facilitated ion transfer. The corresponding transfer mechanism was analyzed in terms of the current–potential profiles, concentration profiles and interfacial distributions, obtained from digital simulations.

1. Introduction

The electrochemical study of ion transfer at the interface between two immiscible electrolyte solutions (ITIES) has allowed determination of relevant thermodynamic and transport parameters, provided that the processes measured are limited by mass diffusion. For the study of kinetic parameters and mechanistic information, the mass transfer rate must be increased. Different experimental approaches have been employed in order to obtain a high mass-transport rate [1,2]. The imposition of a convective flow to increase the mass-transport has also been reported. An electrolyte dropping electrode, analogous to the dropping mercury electrode, has been developed by polarization of the ITIES [3,4]. Other hydrodynamic liquid|liquid cells based on the wall–jet electrode configuration [5] and flow-injection have also been reported [6,7]. Organic gels have been used to stabilize the ITIES in flow [8] and to channel configuration experiments [9,10]. Numerical simulations of ion transfer across ITIES under hydrodynamic conditions in the channel configuration experiments were developed by Jones and Dryfe [11]. An alternative approach to the study of liquid|liquid extraction processes involves the rotating diffusion cell (RDC), introduced by Albery and co-workers [12–14] and modified by Manzanares et al. [15] and Kralj and Dryfe [16] to study the simple and facilitated ion transfer reactions by external polarization. Manzanares et al. [15] have employed an RDC to determine the rate constant of ion transfer kinetics across the thin supported liquid membrane (SLM) between two aqueous phases. Tetrabutylammonium tetrakis-(4-fluorophenyl)-borate, dissolved in 2-nitrophenyl-octylether (NPOE) and used as the organic electrolyte solution supported in a porous membrane (SLM), was put in contact with the aqueous electrolyte. These authors showed that some experimental limitations made the rotating diffusion cell only suitable for the determination of a limited range of standard rate constant values. Moreover, this method requires an accurate evaluation of the different contributions to ion permeability.

Hydrodynamic voltammetry was also reported at ITIES, using an RDC configuration. The voltammetry arises from laminar flow, induced in the organic and aqueous phases of the ITIES, separately. The ITIES has been stabilized by a polyester track-etched membrane material. This methodology has been used to determine reaction mechanisms and kinetic parameters for reactions involving liquid|liquid interfaces [16]. Then, this alternative procedure was extended to the study of facilitated transfer of sodium by dibenzo-18-crown-6 (DB18C6) across the water|1,2-dichloroethane interface [17]. Finally, Fujii et al. [18] performed measurements of ion transfer reaction at a rotating liquid membrane disk electrode (LMDE) and a rotating liquid membrane ring-liquid membrane disk electrode (LMRE-LMDE). These authors have evaluated the ion transfer kinetics and the analytical applications of these methodologies.

Micro liquid|liquid interfaces are useful to study ion transfer reactions because the diffusion fields are controlled by the geometry

* Corresponding author. Tel./fax: +54 351 4334188.
E-mail address: sdassie@mail.fcq.unc.edu.ar (S.A. Dassie).

1572-6657/$ - see front matter © 2011 Elsevier B.V. All rights reserved.
doi:10.1016/j.jelechem.2011.11.028

of the system and because the ohmic potential drop is minimized. These are small-sized interfaces, with low charging current and high mass-transfer rate necessary for fast kinetic measurements. About 30 years ago, Taylor and Girault [19] and Senda and co-workers [20] introduced micrometer-sized liquid|liquid interface (μ-ITIES) supported at the tip of a glass micro-pipette or within a micro-hole made in a thin membrane (supporting film) using the ablation laser technique [21].

μ-ITIES supported at the tip of a micro-pipette can be used to provide spherical diffusion patterns similar to those observed at solid ultra-microelectrodes. This enhanced mass transport produces a steady-state current when the transferring species enters the pipette, whereas classical linear diffusion behavior is observed when the ion exits the pipette. Ion transfer reactions at the micro-pipette are characterized by an asymmetric diffusion regime. The transfer of ions from the micro-pipette to the interface (egress transfer) is controlled by linear diffusion, whereas the transport of ions from outside the pipette to the surface (ingress transfer) is controlled by a cylindrical diffusion field. These two different processes can be easily distinguished during cyclic voltammetric experiments, as the egress and ingress transfers lead to a peak-shaped current response and to a steady-state current respectively [22,23].

On the other hand, Wilke et al. [24] have proposed an alternative methodology consisting in alternately stirring the aqueous or organic phase during the potential sweep to elucidate ion transfer mechanisms across ITIES. The advantages and possibilities of controlling the convective flux of species towards the interface in either the organic or aqueous phase were analyzed using two well-known transfer processes: the simple transfer of tetraethylammonium (TEA^+) and the facilitated transfer of K^+ assisted by DB18C6. In this experimental setup, the convective flux in one phase produced an asymmetry of the diffusion field, that is, a selective decrease in the thickness of the diffusion layer on one side of the interface. This allows distinguishing the direction of the ion transfer. This methodology has been previously used to elucidate the mechanism of the electrochemical transfer of a hydrophilic arenediazonium ion (Fast Red TR) followed by the azo-coupling reaction in the organic phase with 1-naphthylamine, a lipophilic reactant [25]. Lately, we have employed this methodology in order to determine the predominant transfer mechanism of several compounds belonging to tetracyclines [26] or tylosin A [27], and its correspondingly acid-degraded products.

In this work, we present the general equations for a model that describes ion transfer reactions across the oil|water interface assisted by a neutral ligand, under forced hydrodynamic conditions. Analysis is mainly focused on the effect of mechanical stirring of the aqueous or organic phase during the potential sweep, and its influence on the limiting diffusion currents. The model was solved numerically using explicit finite difference and the results of digital simulations were obtained for simple and facilitated ion transfer. The transfer mechanism was analyzed in terms of the current–potential profiles, concentration profiles and interfacial distributions, obtained from digital simulations.

1.1. Theory

In order to derive the current–potential equation using simulation for the transfer of M^{z+} assisted by a neutral ligand (L), where the ion can be complexed by s-ligands in organic (o) and aqueous (w) phases, the following assumptions are made:

(a) The interface between the aqueous and the organic phase is stationary and planar.
(b) Both phases are considered large enough to ensure that the transport of ions through the interface satisfies the semi-infinite condition.
(c) Both phases contain enough inert electrolytes so that migration of the transferring ion can be neglected.
(d) As the rates of the complex formation and dissociation processes are sufficiently large in comparison with the corresponding mass transport rates, complex formation and dissociation are at equilibrium even when current is flowing.
(e) Transfer of all charged species through the interface is reversible. Mass transport occurs in the x coordinate, normal to the interface defined at $x = 0$.
(f) The mass transport caused by forced hydrodynamic conditions is incorporated as a mono-dimensional linear velocity normal to the interface.
(g) The partition coefficient of the neutral species L, $K_{D,L}$, does not depend on the applied potential.
(h) All the charged species are perturbed by the potential applied to the interface and depend on the Nernst equation [28].
(i) Although the activity coefficients are functions of the composition of the solution phase, we neglect the concentration dependence of the activity coefficients for simplicity. All activity coefficients are equal to one.

The complex formation equilibria are the following:

$$\begin{aligned} M^{z+}(\alpha) + L(\alpha) &\rightleftarrows ML^{z+}(\alpha) \\ ML^{z+}(\alpha) + L(\alpha) &\rightleftarrows ML_2^{z+}(\alpha) \\ &\vdots \\ ML_{s-1}^{z+}(\alpha) + L(\alpha) &\rightleftarrows ML_s^{z+}(\alpha) \end{aligned}$$

and the 1:s complex formation constant in the α-phase is defined by:

$$K^{\alpha}_{ML_s^{z+}} = \frac{c^{\alpha}_{ML_s^{z+}}}{c^{\alpha}_{ML^z_{(s-1)}}\, c^{\alpha}_{L}} \tag{1}$$

where α = organic phase (o) or aqueous phase (w) with and $s = 1 \ldots n'$, and $s = 1 \ldots n$ respectively.

The partition coefficient for the neutral species L is defined by:

$$K_{D,L} = \frac{c^{o}_{L}}{c^{w}_{L}} \tag{2}$$

The reversible transfer of ion M^{z+} across the interface between an organic and an aqueous phase is represented by the following equilibrium:

$$M^{z+}(w) \rightleftarrows M^{z+}(o) \tag{R1}$$

The distribution of charged species at the interface is defined by the following Nernst equations:

$$\frac{c^{o}_{species}}{c^{w}_{species}} = \theta_{species}[S_{\lambda}(t)]^{z} \tag{3}$$

where

$$\theta_{species} = \exp\left[\frac{zF}{RT}\left(\Delta^{w}_{o}\phi_{init} - \Delta^{w}_{o}\phi^{o'}_{species}\right)\right] \tag{4}$$

$\Delta^{w}_{o}\phi_{init}$ being the applied potential difference at $t = 0$; $\Delta^{w}_{o}\phi^{o'}_{species}$ the formal potential of each charged species; and

$$S_{\lambda}(t) = \begin{cases} \exp(\sigma t) & 0 \leqslant t \leqslant \lambda \\ \exp[\sigma(2\lambda - t)] & t > \lambda \end{cases} \tag{5}$$

being $\sigma = \frac{Fv}{RT}$, v is a sweep rate, the switching time $\lambda = \frac{t_c}{2}$ where t_c is the total time of the experiment, F the Faraday constant, T the absolute temperature and R the gas constant.

To simulate a voltammogram for a reversible charge transfer under forced hydrodynamic conditions, or controlled stirring, it is necessary to describe the transport of species toward the interface using the following one-dimensional equation:

$$\frac{\partial c^{\alpha}_{\text{species}}(x,t)}{\partial t} = D^{\alpha}_{\text{species}} \frac{\partial^2 c^{\alpha}_{\text{species}}(x,t)}{\partial x^2} - v^{\alpha}_{x} \frac{\partial c^{\alpha}_{\text{species}}(x,t)}{\partial x} \tag{6}$$

where x is the position in the direction normal to the interface, which is located at $x = 0$. $D^{\alpha}_{\text{species}}$ is the diffusion coefficient for α-phase for each species L, M^{z+}, ML_s^{z+} and v^{α}_{x} is the convection velocity of the α-phase, i.e. the rate at which a volume element moves in solution and is responsible for the flow of species from and toward the interface. In the proximity of the rotating-disk electrode, a convective velocity, v^{α}_{x}, independent of the distance, is not a realistic approximation especially for high convective velocities [29,30]. Levich [29] solved the Navier–Stokes and continuity equations for the convective diffusion to the surface of a rotating-disk electrode and developed the solution of the axial velocity component, v^{α}_{x}, as a function of the distance to the electrode. It shows that at long distances from the rotating-disk electrode, the axial velocity component reaches a constant value equal to $0.88447 \times \sqrt{\nu\omega}$, where ν is the kinematic viscosity and ω is the angular velocity of rotation. In the model worked out in this section, the studied electrochemical interface (liquid|liquid interface) is at long distance from the rotating stirrer, which produces forced hydrodynamic conditions. The hydrodynamic conditions produced by the rotating stirrer are comparable to those of the rotating-disk electrode proposed by Levich [29] at long distance. Therefore, our model assumption that the convective velocity, v^{α}_{x}, does not depend on the distance in the proximity of the liquid|liquid interface is a good approximation. Additionally, the present model is developed for low convective velocities. Taking into account that experimental v^{α}_{x} values range between 5×10^{-4} cm s^{-1} (natural convection) and 2×10^{-2} cm s^{-1} (rotating-disk electrode at ω = 10,000 rpm) [31], we have employed an appropriate interval of v^{α}_{x} values in order to ensure a correct physical representation of mass transport phenomena.

According to the boundary conditions, the fluxes of species across the interface ($x = 0$) are expressed by:

$$D^{\text{w}}_{M^{z+}} \frac{\partial c^{\text{w}}_{M^{z+}}(0,t)}{\partial x} + \sum_{s=1}^{n} D^{\text{w}}_{ML_s^{z+}} \frac{\partial c^{\text{w}}_{ML_s^{z+}}(0,t)}{\partial x} = D^{\text{o}}_{M^{z+}} \frac{\partial c^{\text{o}}_{M^{z+}}(0,t)}{\partial x} + \sum_{s=1}^{n'} D^{\text{o}}_{ML_s^{z+}} \frac{\partial c^{\text{o}}_{ML_s^{z+}}(0,t)}{\partial x} \tag{7}$$

$$D^{\text{w}}_{\text{L}} \frac{\partial c^{\text{w}}_{\text{L}}(0,t)}{\partial x} + \sum_{s=1}^{n} sD^{\text{w}}_{ML_s^{z+}} \frac{\partial c^{\text{w}}_{ML_s^{z+}}(0,t)}{\partial x} = D^{\text{o}}_{\text{L}} \frac{\partial c^{\text{o}}_{\text{L}}(0,t)}{\partial x} + \sum_{s=1}^{n'} sD^{\text{o}}_{ML_s^{z+}} \frac{\partial c^{\text{o}}_{ML_s^{z+}}(0,t)}{\partial x} \tag{8}$$

The initial concentration of all species, in all boxes in each α-phase, may be calculated at $t = 0$, where $S_{\lambda}(0) = 1$, as a function of the total initial concentration of cation ($c^{\text{init}}_{MX_z,w}$) and the total initial concentration of ligand ($c^{\text{init}}_{\text{L,o}}$) introduced into the system [32–34]:

$$\begin{cases} c^{\text{init}}_{MX_z,w} = c^{\text{w}}_{M^{z+}}(x,0) + \sum_{s=1}^{n} c^{\text{w}}_{ML_s^{z+}}(x,0) + r\left(c^{\text{o}}_{M^{z+}}(x,0) + \sum_{s=1}^{n'} c^{\text{o}}_{ML_s^{z+}}(x,0)\right) \\ rc^{\text{init}}_{\text{L,o}} = c^{\text{w}}_{\text{L}}(x,0) + \sum_{s=1}^{n} sc^{\text{w}}_{ML_s^{z+}}(x,0) + r\left(c^{\text{o}}_{\text{L}}(x,0) + \sum_{s=1}^{n'} sc^{\text{o}}_{ML_s^{z+}}(x,0)\right) \end{cases} \tag{9}$$

where $r = \frac{V_{\text{o}}}{V_{\text{w}}}$, since V_{o} and V_{w} are the organic and aqueous phase volumes respectively. Rewriting the system of equations (Eq. (9)) as a function of $c^{\text{w}}_{M^{z+}}(x,0)$ and $c^{\text{w}}_{\text{L}}(x,0)$, and considering that the initial potential value is fixed at the distribution potential, $\Delta^{\text{w}}_{\text{o}}\phi_{\text{eq}}$, the following equations are obtained:

$$\begin{cases} c^{\text{init}}_{MX_z,w} = c^{\text{w}}_{M^{z+}}(x,0)\left[1 + r\theta_{M^{z+},\text{eq}}\right] + c^{\text{w}}_{M^{z+}}(x,0) \sum_{s=1}^{n} \left(\prod_{i=1}^{s} K^{\text{w}}_{ML_i^{z+}}\right) \left[c^{\text{w}}_{\text{L}}(x,0)\right]^s + \\ rc^{\text{w}}_{M^{z+}}(x,0) \sum_{s=1}^{n'} \left(\prod_{i=1}^{s} K^{0}_{ML_i^{z+}}\right) \theta_{M^{z+},\text{eq}} (K_{D,\text{L}})^s \left[c^{\text{w}}_{\text{L}}(x,0)\right]^s \\ rc^{\text{init}}_{\text{L,o}} = c^{\text{w}}_{\text{L}}(x,0)[1 + rK_{D,\text{L}}] + c^{\text{w}}_{M^{z+}}(x,0) \sum_{s=1}^{n} s \left(\prod_{i=1}^{s} K^{\text{w}}_{ML_i^{z+}}\right) \left[c^{\text{w}}_{\text{L}}(x,0)\right]^s + \\ rc^{\text{w}}_{M^{z+}}(x,0) \sum_{s=1}^{n'} s \left(\prod_{i=1}^{s} K^{0}_{ML_i^{z+}}\right) \theta_{M^{z+},\text{eq}} (K_{D,\text{L}})^s \left[c^{\text{w}}_{\text{L}}(x,0)\right]^s \end{cases} \tag{10}$$

where $\theta_{M^{z+},eq} = \exp\left[\frac{zF}{RT}\left(\Delta^{\text{w}}_{\text{o}}\phi_{\text{eq}} - \Delta^{\text{w}}_{\text{o}}\phi^{o'}_{M^{z+}}\right)\right]$ (with $\Delta^{\text{w}}_{\text{o}}\phi_{\text{ini}} = \Delta^{\text{w}}_{\text{o}}\phi_{\text{eq}}$ in eq. (4)). The calculation of the distribution potential for this system is developed in Appendix A [35–38].

Other boundary conditions are the following:

$$\text{at } x \to \infty \quad c^{\text{w}}_{\text{species}}(x,t) = c^{\text{w}}_{\text{species}}(x,0) \tag{11}$$

and

$$\text{at } x \to -\infty \quad c^{\text{o}}_{\text{species}}(x,t) = c^{\text{o}}_{\text{species}}(x,0) \tag{12}$$

To solve this system, we employed the explicit finite-difference method for time and distance [39–43].

In addition, the aqueous and the organic phases are divided into boxes with the distance increasing positively from the interface to the bulk of aqueous phase. The net flux at each boundary box, for every species, defines the change in the number of mole inside the box at each time interval.

Taking into account that mass transport may occur by diffusion and convection, it is necessary to select the optimal time and space intervals for each simulated condition. Therefore, time and space were divided into subintervals defined as follows:

$$\Delta t = \min\left[2D^{\alpha}_{\text{max}}\left(\frac{Pe}{v^{\alpha}_{x,\text{max}}}\right)^2, \delta t^{\text{diffusional}}_{\text{converg}}\right] \tag{13}$$

and

$$\Delta x = \sqrt{\frac{D^{\alpha}_{\text{max}}}{D_{\text{M}}}\Delta t} \tag{14}$$

Pe being Péclet number; D^{α}_{max} and $v^{\alpha}_{x,\text{max}}$ are the highest values of the diffusion coefficients and convection velocity, respectively. D_{M} is the model diffusion coefficient, whose optimized value is 0.45 to ensure that the mean free path of particles in the system does not exceed Δx. To compute the values of time discretization, Δt, a minimum value between the following approaches is considered: $\Delta t = 2D^{\alpha}_{\text{max}}\left(\frac{Pe}{v^{\alpha}_{x,\text{max}}}\right)^2$, with $Pe = 0.01$, or $\Delta t = \delta t^{\text{diffusional}}_{\text{converg}} = 1 \times 10^{-5}$ s. This type of discretization guarantees convergence of the current–potential profiles obtained in this work.

For each time interval, the main global process can be divided into three different simultaneous steps: interfacial transfer of ions, mass transport including diffusion and convection, and chemical reactions.

Applying the explicit finite-difference method to Eqs. (7) and (8) the following expression is obtained:

$$\begin{cases} 0 = c^{w}_{M^{z+}}(0,k)\{D^{w}_{M^{z+}} + D^{0}_{M^{z+}}[s_\lambda(t)]^z\} + c^{w}_{M^{z+}}(0,k)\sum_{s=1}^{n} D^{w}_{ML_s^{z+}}\left(\prod_{i=1}^{s} K^{0}_{ML_i^{z+}}\right)[c^{w}_{L}(0,k)]^s + \\ c^{w}_{M^{z+}}(0,k)\sum_{s=1}^{n'} D^{0}_{ML_s^{z+}}\left(\prod_{i=1}^{s} K^{0}_{ML_i^{z+}}\right)\theta_{M^{z+}}[s_\lambda(t)]^z (K_{D,L})^s [c^{w}_{L}(0,k)]^s - \\ D^{w}_{M^{z+}} c^{w}_{M^{z+}}(1,k) - D^{0}_{M^{z+}} c^{0}_{M^{z+}}(1,k) - \sum_{s=1}^{n} D^{w}_{ML_s^{z+}} c^{w}_{ML_s^{z+}}(1,k) - \sum_{s=1}^{n'} D^{0}_{ML_s^{z+}} c^{0}_{ML_s^{z+}}(1,k) \\ 0 = c^{w}_{L}(0,k)[D^{w}_{L} + D^{0}_{L} K_{D,L}] + c^{w}_{M^{z+}}(0,k)\sum_{s=1}^{n} sD^{w}_{ML_s^{z+}}\left(\prod_{i=1}^{s} K^{0}_{ML_i^{z+}}\right)[c^{w}_{L}(0,k)]^s + \\ c^{w}_{M^{z+}}(0,k)\sum_{s=1}^{n'} sD^{0}_{ML_s^{z+}}\left(\prod_{i=1}^{s} K^{0}_{ML_i^{z+}}\right)\theta_{M^{z+}}[s_\lambda(t)]^z (K_{D,L})^s [c^{w}_{L}(0,k)]^s - \\ D^{w}_{L} c^{w}_{L}(1,k) - D^{0}_{L} c^{0}_{L}(1,k) - \sum_{s=1}^{n} sD^{w}_{ML_s^{z+}} c^{w}_{ML_s^{z+}}(1,k) - \sum_{s=1}^{n'} sD^{0}_{ML_s^{z+}} c^{0}_{ML_s^{z+}}(1,k) \end{cases} \quad (15)$$

where $c^{\alpha}_{species}(0,k)$ and $c^{\alpha}_{species}(1,k)$ represent the concentration of species in the interface and in the first box in α-phase, respectively, k being the time step counter.

The mass transport equations for all species in the aqueous and organic phases (Eq. (6)) may be converted to the finite difference form shown below:

$$c^{\alpha}_{species}(1,k+1) - c^{\alpha}_{species}(1,k) = \frac{D^{\alpha}_{species}\Delta t}{(\Delta x)^2}\left[c^{\alpha}_{species}(2,k) - 3c^{\alpha}_{species}(1,k) + 2c^{\alpha}_{species}(0,k)\right] - \frac{v^{\alpha}_{x}\Delta t}{\Delta x}\left[c^{\alpha}_{species}(2,k) - c^{\alpha}_{species}(1,k)\right] \quad (16)$$

for $j = 1$ and

$$c^{\alpha}_{species}(j,k+1) - c^{\alpha}_{species}(j,k) = \frac{D^{\alpha}_{species}\Delta t}{(\Delta x)^2}\left[c^{\alpha}_{species}(j+1,k) - 2c^{\alpha}_{species}(j,k) + c^{\alpha}_{species}(j-1,k)\right] - \frac{v^{\alpha}_{x}\Delta t}{\Delta x}\left[c^{\alpha}_{species}(j+1,k) - c^{\alpha}_{species}(j,k)\right] \quad (17)$$

for $j \geqslant 2$, j being the space step counter.

With this expression the concentrations of each species in each phase may be obtained for j-box as the result of the mass transport, taking into account the diffusion and convection. Although the mass transport is coupled with homogeneous complex equilibria in both phases, to solve the model we considered these processes uncoupled. These equilibria are solved considering each volume element independently [33,34].

In both phases, the mass balance for the ligand and the cation can be defined as follows:

$$\begin{cases} c^{\alpha}_{M^{z+},box} = c^{\alpha}_{M^{z+}}(j,k) + \sum_{s=1}^{n\,or\,n'} c^{\alpha}_{ML_s^{z+}}(j,k) \\ c^{\alpha}_{L,box} = c^{\alpha}_{L}(j,k) + \sum_{s=1}^{n\,or\,n'} s c^{\alpha}_{ML_s^{z+}}(j,k) \end{cases} \quad (18)$$

where $c^{\alpha}_{species,box}(j,k)$ is the total species concentration in the j-box in the α-phase.

Rewriting the system of equations (eq. (18)) as a function of $c^{\alpha}_{M^{z+}}(j,k)$ and $c^{\alpha}_{L}(j,k)$, the following equations are obtained:

$$\begin{cases} c^{\alpha}_{M^{z+},box} = c^{\alpha}_{M^{z+}}(j,k) + c^{\alpha}_{M^{z+}}(j,k)\sum_{s=1}^{n\,or\,n'}\left(\prod_{i=1}^{s} K^{\alpha}_{ML_i^{z+}}\right)[c^{\alpha}_{L}(j,k)]^s \\ c^{\alpha}_{L,box} = c^{\alpha}_{L}(j,k) + c^{\alpha}_{M^{z+}}(j,k)\sum_{s=1}^{n\,or\,n'} s\left(\prod_{i=1}^{s} K^{\alpha}_{ML_i^{z+}}\right)[c^{\alpha}_{L}(j,k)]^s \end{cases} \quad (19)$$

A modification of the Powell hybrid method [44–46] was used to find the roots of all equation systems (Eqs. (10), (15), and (19)).

Once interfacial concentrations have been calculated for each species, the total current can be computed as in Eq. (20):

$$I(t) = \frac{zFA}{0.5\Delta x}\left[D^{\alpha}_{M^{z+}}\left(c^{\alpha}_{M^{z+}}(1,t) - c^{\alpha}_{M^{z+}}(0,t)\right) + \sum_{s=1}^{n\,or\,n'} D^{\alpha}_{ML_s^{z+}}\left(c^{\alpha}_{ML_s^{z+}}(1,t) - c^{\alpha}_{ML_s^{z+}}(0,t)\right)\right] \quad (20)$$

2. Results and discussion

The results are presented in two subsections according to the model developed in Section 1.1 for a general system. Section 2.1 shows results obtained for simple ion transfer and Section 2.2 is devoted to the analysis of the different facilitated ion transfer mechanisms. Selected systems with varying degrees of complexity are discussed, starting with the simple ion transfer.

The following parameters are fixed for all the simulations present in this section:

$T = 298.15$ K, $F = 96{,}485$ C mol^{-1}, $R = 8.314$ J K^{-1} mol^{-1}, $v = 0.050$ V s^{-1}; $D^{w}_{species} = 1.0 \times 10^{-5}$ cm^2 s^{-1}; $\xi = \sqrt{D^{o}_{species}/D^{w}_{species}} = 1.12$ for the H_2O|1,2-DCE system [47] and $A = 1.0$ cm^2.

2.1. Simple transfer of M^+ across a liquid|liquid interface

The model presented allows simulating several different systems. In the first place, we analyze the simple ion transfer across a liquid|liquid interface.

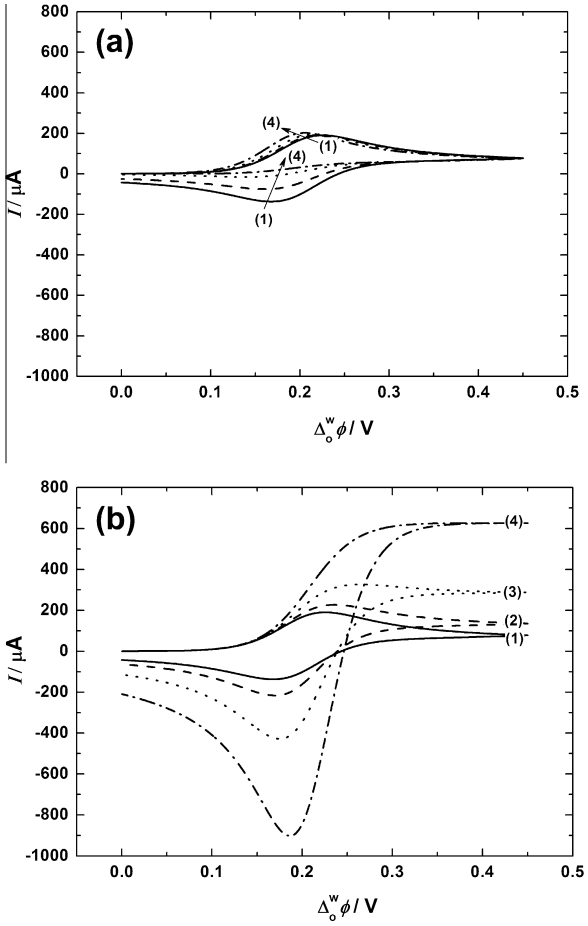

Fig. 1. Voltammograms at different forced hydrodynamic conditions for the simple transfer of M^+. Without convection (1), with $v^{\alpha}_{x} = 1 \times 10^{-3}$ cm s^{-1} (2), $v^{\alpha}_{x} = 3 \times 10^{-3}$ cm s^{-1} (3) and $v^{\alpha}_{x} = 7 \times 10^{-3}$ cm s^{-1} (4) with α = o in panel (a) and with α = w in panel (b). Simulation parameters: $\Delta^{w}_{o}\phi^{o'}_{M^+} = 0.20$ V and $c^{init}_{MX,w} = 1 \times 10^{-3}$ M.

This simple system is useful to show how the application of forced hydrodynamic conditions at a particular phase allows modifying diffusion-controlled voltammograms, concentrations profiles and interfacial ion distributions.

Considering a monovalent cation ($z = 1$) which does not form complexes in the organic or aqueous phase ($n = n' = 0$), the simple ion transfer can be represented by:

$$M^+(w) \rightleftarrows M^+(o) \tag{25}$$

First, we analyze the effect of forced hydrodynamic conditions on the current–potential profiles while only the organic or the aqueous phases are alternately stirred. Fig. 1a shows voltammograms obtained while only the organic phase is stirred, in comparison with voltammograms obtained with both phases in quiescent conditions. When the convective velocity in the organic phase, v_x^o, is increased, a progressive decrease in the peak current value during the backward sweep is observed. This behavior is due to the fact that M^+ transferred to the organic phase is removed from the proximity of interface by convection. Consequently its concentration gradient decreases and the current also diminishes. It is important to note that the free energy of the charge transfer process is favoured when the convective velocity is increased, therefore in the forward sweep the peak current occurs at lower potential values. On the other hand, when only the aqueous phase is stirred (Fig. 1b), the positive (I^+_{peak}) and negative peak current (I^-_{peak}) values show important changes associated with convective velocity. Comparing this signal with the electrochemical response obtained for unstirred solution, a stationary current in the forward sweep and a higher peak current in the backward sweep are observed. The rate of mass transfer of the ion present in the aqueous phase is enhanced with stirring and a limiting current is reached if v_x^w is higher enough. The shape of the backward current–potential profile is diffusion-like, but as the amount of substance transferred to the organic phase is higher, I^-_{peak} is larger.

Other important information that can be obtained by digital simulations relates to concentration profiles at, or near to, the interface at a fixed potential value. The effect of the convective velocity on the charge transfer process can be explained using these profiles.

Fig. 2 shows the concentration profiles of M^+ as function of the distance to the interface at two different fixed potential values. In Fig. 2a and b the selected potential value corresponds to the switching time. In the first case, when ions are transferred from the aqueous to the organic phase, while the last one is stirred (Fig. 2a), a decrease in the organic M^+ concentration profile is observed whereas the aqueous M^+ concentration profile remains unchanged. These results describe that the transferred ions are removed from the organic side of the interface to the bulk of the organic phase. Digital simulation results obtained when the aqueous phase is stirred (Fig. 2b) reveal that the aqueous diffusion layer thickness decreases and the interfacial concentration of M^+ in the organic side of the interfacial region increases, i.e. $c^o_{M^+}(0,t) > c^{init}_{MX_z,w}$. In Fig. 2c and d, concentration profiles at a selected potential value on the backward scan, $\Delta^w_o\phi = 0.20$ V, are shown. If the organic phase is stirred, a decrease in both concentration profiles is found (Fig. 2c), while a notable accumulation of M^+ in the organic phase near the interface occurs as a consequence of the convection applied to the aqueous phase (Fig. 2d).

Another tool provided by digital simulation involves the interfacial distributions in the aqueous and organic side of the interface during the whole potential sweep. Fig. 3a shows the interfacial distribution of M^+ for quiescent and organic stirred solutions. For quiescent solutions, the interfacial concentration of M^+ in the aqueous side, at the beginning of the potential sweep, is equal to the analytical concentration. According to the direction of potential sweep and the transfer ions, the concentration of M^+ in the organic side increases but cannot equal the analytical concentration because the ions are transported from the interface to the bulk of the organic phase faster than in the aqueous phase. When the organic phase is

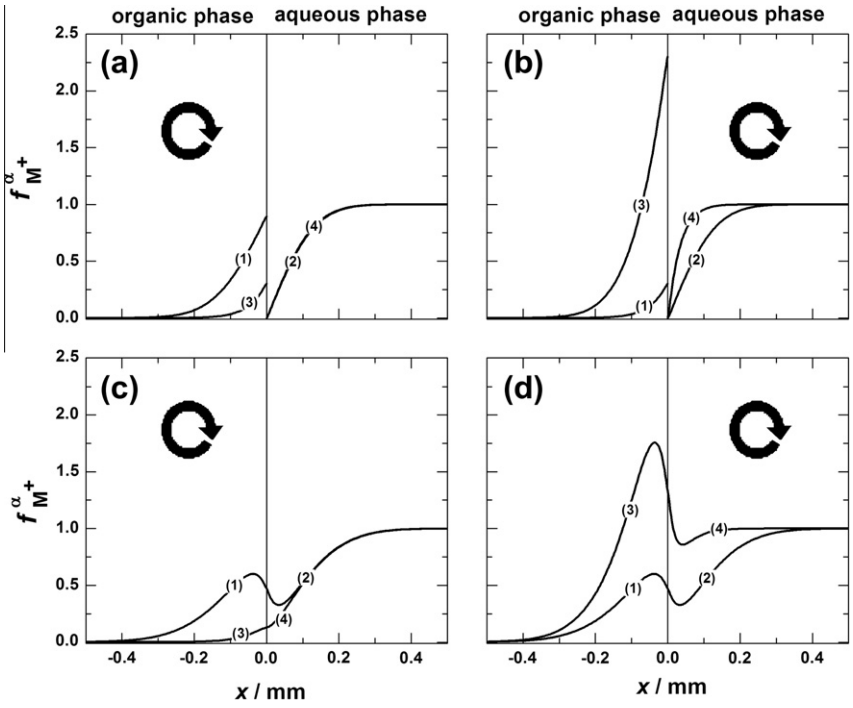

Fig. 2. Concentration profiles as a function of the distance to the liquid|liquid interface ($x = 0$) at two different potential values: $\Delta^w_o\phi = 0.45$ V (a) and (b), and $\Delta^w_o\phi = 0.20$V (at the backward potential sweep) (c) and (d). Normalized concentrations of M^+ in the organic phase $\left(f^o_{M^+} = c^o_{M^+}\left(c^{init}_{MX,w}\right)^{-1}\right)$ and M^+ aqueous phase $\left(f^w_{M^+} = c^w_{M^+}\left(c^{init}_{MX,w}\right)^{-1}\right)$. Without convection: $f^o_{M^+}$ (1) and $f^w_{M^+}$ (2) and with forced hydrodynamic conditions ($v^{\alpha}_x = 3 \times 10^{-3}$ cm s^{-1} with $\alpha = o$ in panels (a) and (c) and with $\alpha = w$ in panels (b) and (d)): $f^o_{M^+}$ (3) and $f^w_{M^+}$ (4). Other simulation parameters as in Fig. 1.

stirred, the interfacial concentration of M^+ in the organic side reaches a maximum value in the forward potential sweep which is lower than the maximum which corresponds to the quiescent solutions. This behavior is due to the difference between the ion arrival rate by the transfer process, and the ion removal rate by the stirring of the phase. As this difference is negative, the interfacial concentration of M^+ has a value lower than that for the process without forced hydrodynamic conditions. In the forward potential sweep, the interfacial concentration of M^+ in the aqueous side shows a decrease at lower potential values than for unstirred solutions. This is because the convection in the organic phase forces a removal of ions from the organic side of the interface, promoting the transfer of more ions. Therefore, for the organic stirred solutions in the backward potential sweep, the interfacial concentration of M^+ in the organic side decreases monotonously, while the interfacial concentration of M^+ in the aqueous side increases but never reaches the analytical concentration. Generally, convection is responsible for distributing ions from the interface to the bulk of the phases. Thus, it is not possible to recover all the charge transferred species in the forward potential sweep. Fig. 3b shows the distribution profiles when aqueous phase is stirred. In the forward potential sweep the interfacial concentration of M^+ in the aqueous side decreases at higher potential values than for unstirred solutions. Furthermore, the interfacial concentration of M^+ in the organic side increases to reach a maximum that exceeds the bulk concentration of M^+ in aqueous solution. This occurs due to M^+ transfer to organic phase is accumulated near the interface, because the mass transport in the organic phase is diffusion-controlled. The increase in the ion interfacial concentration continues in the backward potential sweep to reach a maximum (around 0.25 V), and from this potential value, the M^+ concentration in the organic side decreases with a marked slope and, concomitantly, the cation concentration in the aqueous side increases. This increase reaches a maximum concentration value which is lower than that of the M^+ concentration in the organic side because the convection in aqueous phase removes ions from the interface toward the bulk of the aqueous phase.

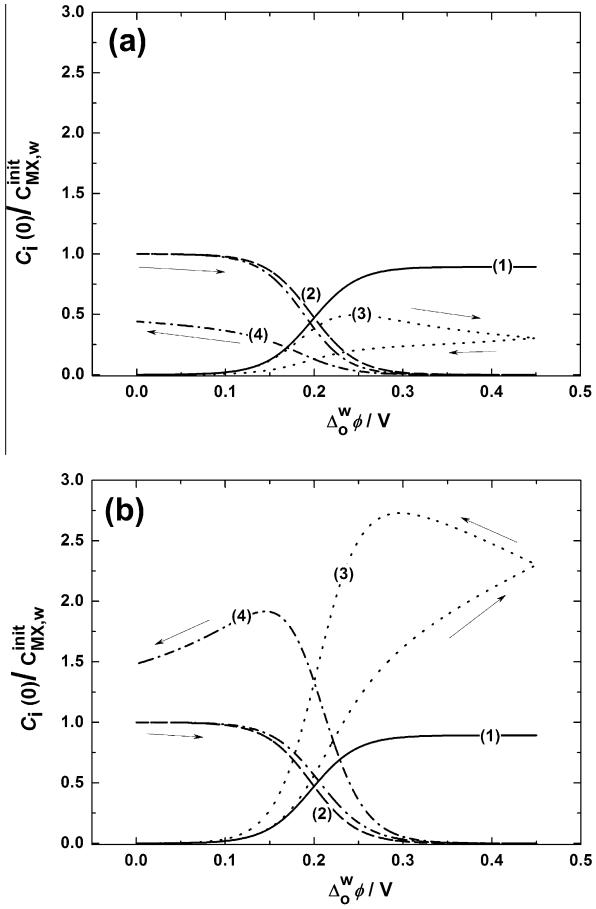

Fig. 3. Interfacial distribution of M^+ during the potential scanning. Normalized concentrations of M^+ in the organic phase ($f^o_{M^+}$) and M^+ aqueous phase ($f^w_{M^+}$). Without convection: $f^o_{M^+}$ (1) and $f^w_{M^+}$ (2) and with forced hydrodynamic conditions ($v^\alpha_x = 3\times10^{-3}$ cm s^{-1} with α = o in panel (a) and with α = w in panel (b)): $f^o_{M^+}$ (3) and $f^w_{M^+}$ (4). Other simulation parameters as in Fig. 1a.

2.2. Facilitated ion transfer across liquid|liquid interface. Elucidation of charge transfer mechanisms

The aim of this section is to develop a methodology for the determination of the charge transfer mechanisms for the facilitated ion transfer by the application of forced hydrodynamic conditions in the organic or aqueous phases.

The simulated system presented in this section is the transfer of M^+ assisted by a neutral ligand, L, where $z = 1$ and $s = 1$. Our model contemplates the formation of the complex ML^+. M^+ is initially present in aqueous phase and L in organic phase, L being a hydrophobic ligand ($K_{D,L} \gg 1$).

Two possible mechanisms of facilitated ion transfer are considered in this work. One is called TIC/TID (transfer by interfacial complexation/decomplexation) in which the complex ML^+ is formed interfacially; the other is called ACT (aqueous complexation reaction followed by transfer) in which the complex is formed in aqueous phase and is then transferred to the organic phase [48]. Particularly, both global mechanisms differ in their aqueous formation constant values, $K^w_{ML^+}$. It is important to note that both TIC/TID and ACT mechanisms are emerging mechanisms of the model, i.e. these overall reactions were not explicitly incorporated in the model (see Section 1.1).

2.2.1. Mass transport: convection and diffusion

The effect of including the convection in mass transport is particularly notable in the shape of the voltammograms shown in Fig. 4. Based on the change of electrochemical signals, the mechanism of facilitated ion transfer can be elucidated if the system is studied in the optimal experimental conditions. This can be carried out by answering the following key questions: what is the species that limits the current? And what is the phase being stirred?

When $c^{init}_{MX,w} \gg c^{init}_{L,o}$ and a TIC/TID mechanism are considered (Fig. 4a), current–potential profiles corresponding to charge transfer process with forced hydrodynamic condition in aqueous phase present no difference compared with diffusion-controlled process because the phase with an excess of ions is being stirred. Instead, when the organic phase is stirred, the limiting current species (L) is carried to the interface, therefore, the current increases in the forward potential sweep but decreases drastically in the backward potential sweep. This is because the stirring redistributes the formed complex to the bulk of the organic phase. On the other hand, if $c^{init}_{MX,w} \gg c^{init}_{L,o}$ and an ACT mechanism is considered (Fig. 4b), when current–potential profiles corresponding to charge transfer process with forced hydrodynamic condition in aqueous phase is compared with the response in the quiescent solution, a stationary current is observed in the forward potential sweep and a higher current peak in the backward potential sweep. The rate of mass transport of the complex present in the aqueous phase is enhanced with stirring and a limiting current is reached if convective velocity is higher enough. The shape of the backward peak is not affected, but as the amount of substance transferred to the organic phase is higher than that in the absence of convection, the negative peak increases. When the organic phase is stirred, a negligible effect of stirring is observed in the forward potential

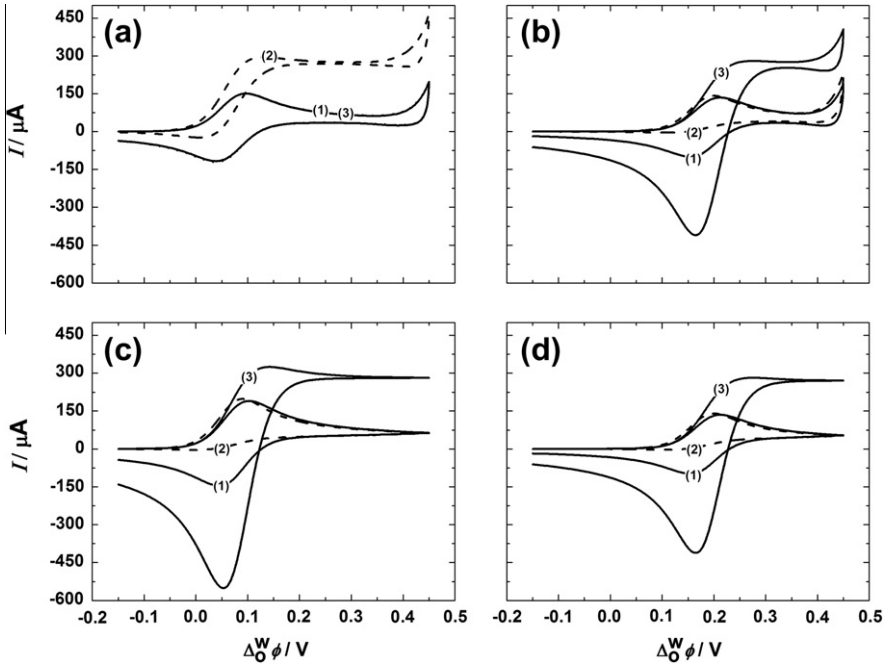

Fig. 4. Voltammograms at different forced hydrodynamic conditions applied to aqueous or organic phase, for different charge transfer mechanisms: TIC/TID (a) and (c), and ACT (b) and (d). Without convection (1), with $v_x^o = 3 \times 10^{-3}$ cm s^{-1} (2) and $v_x^w = 3 \times 10^{-3}$ cm s^{-1} (3). Experimental conditions: $c_{MX,w}^{init} \gg c_{L,o}^{init}$ ($c_{MX,w}^{init} = 1 \times 10^{-1}$ M and $c_{L,o}^{init} = 1 \times 10^{-3}$ M) in panels (a) and (b), and $c_{MX,w}^{init} \ll c_{L,o}^{init}$ ($c_{MX,w}^{init} = 1 \times 10^{-3}$ M and $c_{L,o}^{init} = 1 \times 10^{-1}$ M) in panels (c) and (d). Simulation parameters: $K_{ML^+}^w = 1 \times 10^{-15}$ and $K_{ML^+}^o = 1 \times 10^{10}$ for TIC/TID mechanism, $K_{ML^+}^w = 1 \times 10^5$ and $K_{ML^+}^o = 1 \times 10^{10}$ for ACT mechanism. $D_{M^+}^w = 1 \times 10^{-5}$ cm^2 s^{-1}, $D_L^w = D_{ML^+}^w = 5 \times 10^{-6}$ cm^2 s^{-1}, $\xi = 1.12$ and $\Delta_o^w\phi_{M^+}^{o'} = 0.60$ V.

sweep. This is a clear indication that the transfer process is controlled by the diffusion of the species present in the unstirred aqueous phase. On the other hand, the backward current peak reveals a decrease in the return of species to the aqueous phase. This result is easily explained considering that the ions which reach the organic phase, are removed from the interface by stirring and thus the ions interfacial concentration diminishes.

In contrast, when $c_{MX,w}^{init} \ll c_{L,o}^{init}$ for both mechanisms the voltammograms show the same shape but different values of peak current and transfer potentials (Fig. 4c and d). When aqueous phase is stirred, the peak current increases in the forward and backward potential sweep since the species limiting current (M^+ or ML^+ in TIC and ACT mechanisms, respectively) is present in the aqueous phase.

This information clearly indicates that the first experimental condition ($c_{MX,w}^{init} \gg c_{L,o}^{init}$) allows us to elucidate between TIC and ACT mechanisms, because current–potential profiles present different shapes when the aqueous or organic phase is stirred. Thus, it is possible to distinguish the mechanism of facilitated transfer by choosing the adequate experimental conditions.

As in the ACT mechanism, the ML^+ complex is present initially in the aqueous phase and then is transferred to the organic phase, the electrochemical response looks like a simple transfer of M^+, system analyzed in detail in Section 2.1. The rest of this section is therefore devoted to describing the TIC mechanism thoroughly.

Fig. 5 shows the concentration profiles obtained for quiescent and stirred solutions at the switching time ($\Delta_o^w\phi = 0.45$ V). When $c_{MX,w}^{init} \gg c_{L,o}^{init}$, and a TIC mechanism is considered under forced hydrodynamic conditions applied to the organic phase (Fig. 5a), it can be observed that the thickness of the diffusion layer δ (diffusion path length) depends on the intensity of the convective fluxes. In this sense, the mass transport in the organic phase displays two different behaviors for stirred and quiescent solutions. There is an increased free ligand transport toward the interface, and an increased complex transport from the interface to the bulk of the organic phase. The increase in the transport of free ligand is responsible for the limiting current observed in the forward potential sweep. The absence of current in the backward potential sweep is caused by an increase in the transport of formed complex (see Fig. 4a). For a system with $c_{MX,w}^{init} \ll c_{L,o}^{init}$, for a TIC mechanism under forced hydrodynamic conditions applied to the aqueous phase (Fig. 5b), δ depends on the intensity of the convective fluxes. The forced hydrodynamic conditions produce an increased mass transport toward the interface and an accumulation of the complex formed in the organic side of the interface. The first behavior is responsible for the limiting current observed in the forward potential sweep and the complex accumulation produces a large current in the backward potential sweep (see Fig. 4c). In Fig. 5b, it should be noted that the concentration of the complex formed in the organic side of the interface exceeds the analytical concentration of the cation in the aqueous phase.

Fig. 6 shows that the analysis of the species interfacial distribution is a powerful tool for understanding global transfer mechanisms. When $c_{MX,w}^{init} \gg c_{L,o}^{init}$, for a TIC mechanism under forced hydrodynamic conditions applied to organic phase (Fig. 6a), it can be observed that the interfacial concentration of M^+ decreases about 3.5 mM, which is greater than the analytical concentration of L, due to the mass transport from the bulk of the organic phase to the interface. In the backward potential sweep, interfacial M^+ concentration continues decreasing to about 0.15 V when the concentration increases; however, it never reaches the initial concentration because convection in organic phase removes the ML^+ complex from the interface in the forward potential sweep. When the aqueous phase is stirred (Fig. 6b), the interfacial concentration of M^+ decreases about 0.5 mM because cations are pushed to the interface. Before reaching 0.15 V, although the concentration of L is not zero, the concentration of interfacial M^+ increases because the amount of ions pushed to the interface due to convection overcomes the amount of L available to form the complex. At the switching potential, the direct transfer of M^+ is observed. We can also note that the concentration of ML^+ overcomes the concentra-

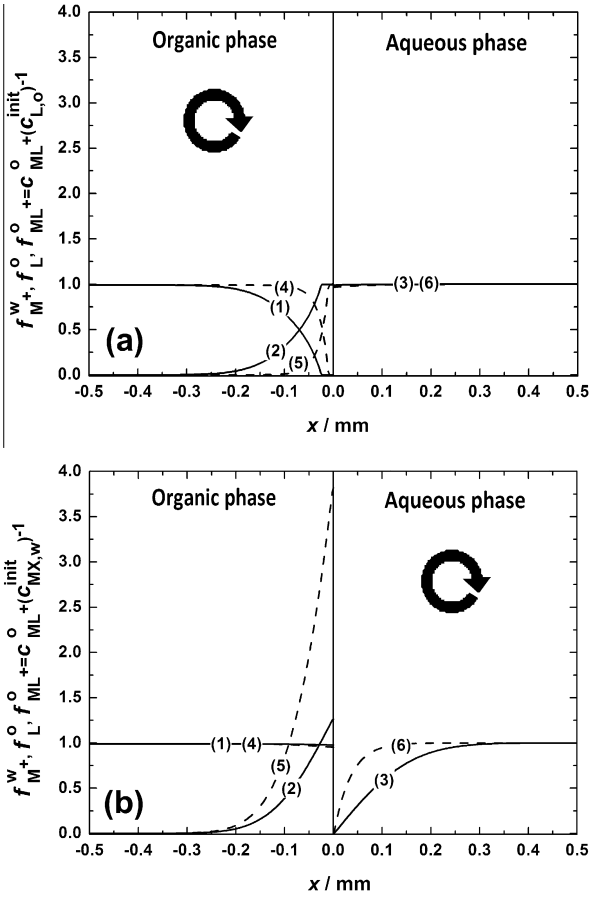

Fig. 5. Concentration profiles as a function of the distance to the liquid|liquid interface ($x = 0$) for the facilitated ion transfer TIC/TID mechanism at $\Delta_o^w\phi = 0.45$ V with hydrodynamic forced conditions in organic (a) and aqueous phase (b). Normalized concentrations of L $\left(f_L^o = c_L^o\left(c_{L,o}^{init}\right)^{-1}\right)$ and ML^+ ($f_{ML^+}^o$) in the organic phase, and M^+ $\left(f_{M^+}^w = c_{M^+}^w\left(c_{MX,w}^{init}\right)^{-1}\right)$ in the aqueous phase. Without convection: f_L^o (1),$f_{ML^+}^o$(2) and $f_{M^+}^w$ (3); and with hydrodynamic forced conditions ($v_x^\alpha = 3\times10^{-3}$ cm s^{-1} with $\alpha =$ o in panel (a) and with $\alpha =$ w in panel (b)): f_L^o (4),$f_{ML^+}^o$(5) and $f_{M^+}^w$ (6). Experimental conditions: $c_{MX,w}^{init} \gg c_{L,o}^{init}$ ($c_{MX,w}^{init} = 1\times10^{-1}$ M and $c_{L,o}^{init} = 1\times10^{-3}$ M) in panel (a) and $c_{MX,w}^{init} \ll c_{L,o}^{init}$ ($c_{MX,w}^{init} = 1\times10^{-3}$ M and $c_{L,o}^{init} = 1\times10^{-1}$ M) in panel (b). Other simulation parameters as in Fig. 4.

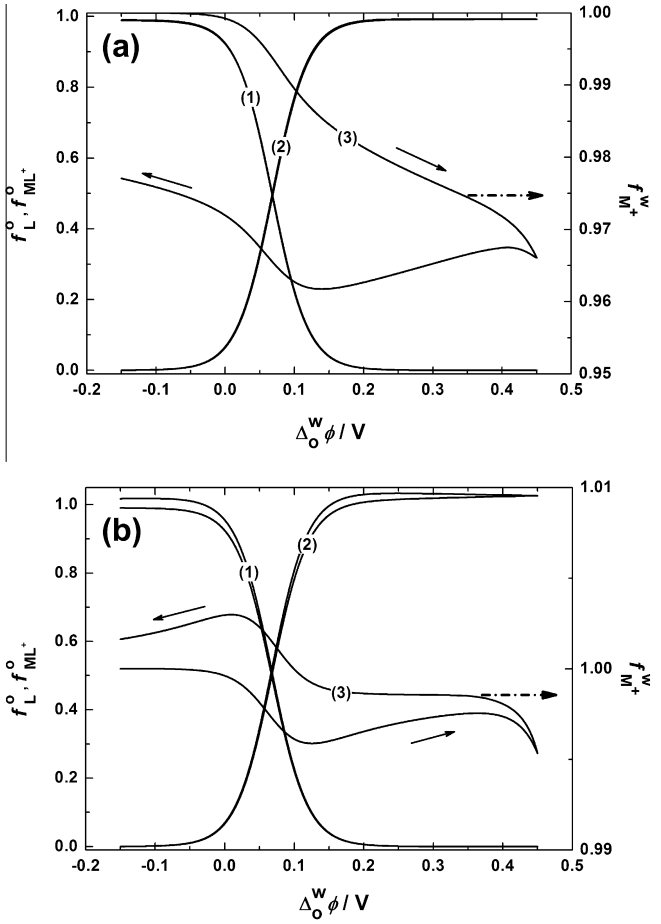

Fig. 6. Interfacial distribution of species during the potential scanning for TIC/TID mechanism with forced hydrodynamic conditions in organic (a) and aqueous phase (b). Normalized interfacial concentrations of f_L^o (1), $f_{ML^+}^o$ (2) and $f_{M^+}^w$ (3). Experimental condition: $c_{MX,w}^{init} \gg c_{L,o}^{init}$($c_{MX,w}^{init} = 1\times10^{-1}$ M and $c_{L,o}^{init} = 1\times10^{-3}$M). Other simulation parameters as in Fig. 4.

tion of species which is in defect, because species in the organic phase are faster than those in the aqueous phase and, in this manner, the excess of M^+ changes the equilibrium of the complex formation to products. In the backward potential sweep, interfacial concentration of M^+ increases overcoming the initial concentration because there is a higher amount of ML^+ to transfer to the aqueous phase and the interfacial concentration of M^+ decreases due to convection.

To summarize the information that emerges from the whole analysis, the peak-to-peak potential difference, $\Delta(\Delta_0^w\phi_{peak})$, can be a helpful tool. In the rest of this section the peak-to-peak potential difference, $\Delta(\Delta_0^w\phi_{peak})$, will be useful as a descriptor of the different limiting current species. In particular, $\Delta(\Delta_0^w\phi_{peak})$ is a specific descriptor of mixed diffusion regimes. Fig. 7 shows the peak-to-peak potential difference as a function of the concentration ratios between ligand and cation. These amounts have been obtained by fixing the initial concentration of cation ($\log(c_{MX,w}^{init}) = -3.00$). This figure also shows the current–potential profiles for quiescent and forced hydrodynamic conditions applied in each phase, in three different experimental conditions.

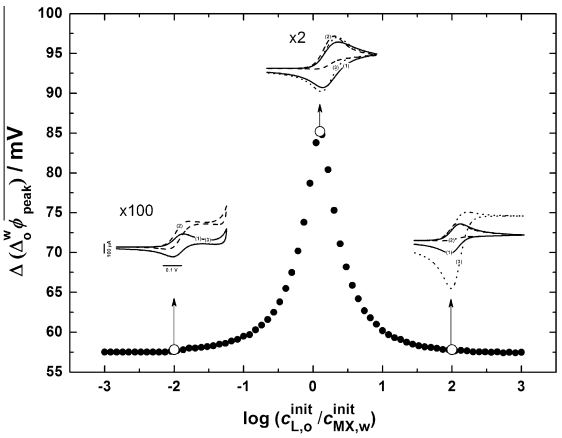

Fig. 7. Peak-to-peak potential separation as a function of the decimal logarithm of the initial concentrations ratio for TIC/TID mechanism. $c_{MX,w}^{init} = 1\times10^{-3}$ M. Voltammograms without convection (1), with forced hydrodynamic conditions $v_x^o = 3\times10^{-3}$ cm s^{-1} (2) and $v_x^w = 3\times10^{-3}$ cm s^{-1} (3). Other simulation parameters as in Fig. 4.

Girault and co-workers [49] have demonstrated that peak-to-peak potential difference depends on the stoichiometry of the complexation, but as in this study 1:1 stoichiometry is chosen, the evolution of the peak-to-peak potential difference is symmetric with respect to $\log(c_{L,o}^{init}/c_{MX,w}^{init}) \simeq 0$. In both limiting $\log(c_{L,o}^{init}/c_{MX,w}^{init})$

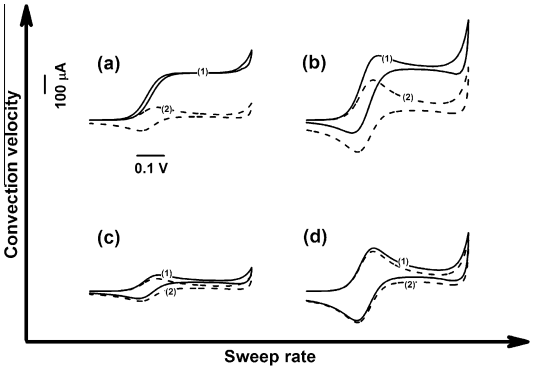

Fig. 8. Effect of sweep rate and convective velocity on voltammograms for TIC/TID mechanism. Experimental condition: $c^{init}_{MX,w} \gg c^{init}_{L,o}$ ($c^{init}_{MX,w} = 1 \times 10^{-1}$ M and $c^{init}_{L,o} = 1 \times 10^{-3}$ M). Convective on organic phase (1) and on aqueous phase (2). $v = 0.010$ V s^{-1} and $v^{\alpha}_x = 3 \times 10^{-3}$ cm s^{-1} (a), $v = 0.100$ V s^{-1} and $v^{\alpha}_x = 3 \times 10^{-3}$ cm s^{-1} (b), $v = 0.010$ V s^{-1} and $v^{\alpha}_x = 5 \times 10^{-4}$ cm s^{-1} (c) and $v = 0.100$ V s^{-1} and $v^{\alpha}_x = 5 \times 10^{-4}$ cm s^{-1} (d). Other simulation parameters as in Fig. 4.

values, $\Delta(\Delta^{w}_{0}\phi_{peak})$ reaches a constant value equal to 59 mV. Between these two well-known limiting cases, the dependence of the peak-to-peak potential difference is intermediate, because the diffusion of both free ion and ligand may limit the transfer, so that a mixed diffusion regime establishes. The evolution of the peak-to-peak difference represented in Fig. 7 reaches a maximum at $\log(c^{init}_{L,o}/c^{init}_{MX,w}) = \frac{1}{2}\log(D^{w}_{M^+}/D^{o}_{L})$. Under conditions of mixed diffusion regime, when only one phase is stirred, the transfer is limited by the species present in the unstirred phase, i.e. when the aqueous phase is stirred, the facilitated ion transfer is controlled by the diffusion of the ligand from the bulk of the organic phase to the interface.

2.2.2. Effect of the sweep rate and the convective velocity

In Fig. 8 the effects of sweep rate and convective velocity on the voltammetric response are compared. All current–potential profiles shown in this figure were obtained for a TIC mechanism with $c^{init}_{MX,w} \gg c^{init}_{L,o}$. The noticeable differences between the stirred and unstirred experiments are observed at low sweep rates and when the current controlling species is present in the phase that is stirred. This result implies that under these experimental conditions the stirring offers the most relevant advantages as a mechanistic tool. It is important to notice that relatively low convective velocities prove enough to cause appreciable changes in the electrochemical signals obtained for stirred and unstirred solutions. Moreover, at low convective velocity, mechanical disturbances on the interface studied are minimized, and the model well represents experimental situations [24]. It is important to emphasize that a good agreement can be found between the results obtained with the presented model and those previously reported in literature for the K^+ transfer assisted by DB18C6 across the H_2O|1,2-dichloroethane interface (see fig. 4b in Ref. [24]).

3. Conclusion

The key aspect in this work is the effect of forced hydrodynamic conditions over the ion transfer across the oil|water interface. General equations were developed for ion transfer and the model was solved using explicit finite difference in time and space. Three charge transfer mechanisms (simple ion transfer, TIC and ACT mechanisms) were systematically analyzed in order to illustrate the effect of the convective velocity on the shape of the current–potential profiles. In the case of the simple ion transfer, the shape of the voltammograms was correlated with the changes observed in the ion interfacial distribution and the concentration profiles.

In addition, a procedure for the determination of the charge transfer mechanisms for the facilitated ion transfer (TIC or ACT mechanisms) based on the application of forced hydrodynamic conditions in the organic or aqueous phases was presented. From the shape of the current–potential profiles it is possible to directly determine the charge transfer mechanism in the appropriate experimental conditions.

TIC mechanism was exhaustively analyzed because the voltammetric behavior depends on the initial concentrations of cation and ligand in the aqueous and organic phase, respectively [49]. Hence, the most important result shown relates to the fact that, under conditions of mixed diffusion regime, when only one phase is stirred, the transfer is limited by the species present in the unstirred phase. Therefore, the shape of the voltammetric signal changes significantly for the different experimental conditions (forced hydrodynamic conditions in the aqueous or organic phase).

In the last section, the effects of sweep rate and convective velocity on the voltammetric response were compared. The most important differences in electrochemical behavior are seen at low sweep rates and when the current controlling species is present in the stirred phase. It is important to observe that relatively low convective velocities are enough to find appreciable changes in the electrochemical signal, and this condition minimizes the mechanical stirring effects on the interface.

Finally, it is important to underline the agreement between the simulated results obtained using the model presented in this work, and the experimental results previously reported in the literature for the simple transfer of TEA^+ and K^+ transfer assisted by DB18C6 across the H_2O|1,2-dichloroethane interface [24].

Acknowledgements

S.A.D. is a researcher from Consejo Nacional de Investigaciones Científicas y Tecnológicas (CONICET). J.M.O. and R.A.F. thank CONICET for the fellowships granted. Financial support from CONICET and Secretaría de Ciencia y Tecnología de la Universidad Nacional de Córdoba (SECyT-UNC) are acknowledged. Help from F. Vega Mercado with the graphical abstract and language assistance by C. Mosconi are gratefully acknowledged.

Appendix A

In this appendix, the general equations are developed for obtaining the distribution potential of the system.

While the simulations presented in this work do not include signals corresponding to the transfer of supporting electrolyte, in the calculation of potential distribution it is necessary to include all species in the system. The initial compositions of the aqueous and organic phase are defined as follows:

The aqueous phase of volume V_w contains two base electrolytes, MX_z and NX.
The organic phase of volume V_o contains a base electrolyte, OY and a neutral ligand, L.
The volume ratio of the two phases is defined as $r = V_o/V_w$.

In both phases the neutral ligand forms complexes only with M^{z+}. The ion-pair formation for all species in the both phases is neglected.

According to the studies of Hung [35,36], Kakiuchi [37] and Garcia et al. [38], the equilibrium concentrations of ionic species and

the distribution potential can be calculated from the initial concentrations of ions, its standard Gibbs energy of transfer, the complex formation constants and the volume ratio of the two phases.

The law of mass conservation of the different species in the system reads as follows:

$$c^{\text{init}}_{\text{MX}_z,w} = c^{\text{w}}_{\text{M}^{z+}} + \sum_{s=1}^{n} c^{\text{w}}_{\text{ML}_s^{z+}} + r\left(c^{\text{o}}_{\text{M}^{z+}} + \sum_{s=1}^{n'} c^{\text{o}}_{\text{ML}_s^{z+}}\right) \tag{A1}$$

$$rc^{\text{init}}_{\text{L,o}} = c^{\text{w}}_{\text{L}} + \sum_{s=1}^{n} sc^{\text{w}}_{\text{ML}_s^{z+}} + r\left(c^{\text{o}}_{\text{L}} + \sum_{s=1}^{n'} sc^{\text{o}}_{\text{ML}_s^{z+}}\right) \tag{A2}$$

$$rc^{\text{init}}_{\text{OY,o}} = c^{\text{w}}_{\text{O}^+} + rc^{\text{o}}_{\text{O}^+} \tag{A3}$$

$$rc^{\text{init}}_{\text{OY,o}} = c^{\text{w}}_{\text{Y}^-} + rc^{\text{o}}_{\text{Y}^-} \tag{A4}$$

$$zc^{\text{init}}_{\text{MX}_z,w} + c^{\text{init}}_{\text{NX,w}} = c^{\text{w}}_{\text{X}^-} + rc^{\text{o}}_{\text{X}^-} \tag{A5}$$

$$c^{\text{init}}_{\text{NX,w}} = c^{\text{w}}_{\text{N}^+} + rc^{\text{o}}_{\text{N}^+} \tag{A6}$$

The conditions of the electroneutrality for each phase are the following:

$$c^{\text{w}}_{\text{O}^+} + c^{\text{w}}_{\text{N}^+} + zc^{\text{w}}_{\text{M}^{z+}} + z\sum_{s=1}^{n} c^{\text{w}}_{\text{ML}_s^{z+}} + c^{\text{w}}_{\text{H}^+} = c^{\text{w}}_{\text{Y}^-} + c^{\text{w}}_{\text{X}^-} + c^{\text{w}}_{\text{HO}^-} \tag{A7}$$

or

$$c^{\text{o}}_{\text{O}^+} + c^{\text{o}}_{\text{N}^+} + zc^{\text{o}}_{\text{M}^{z+}} + z\sum_{s=1}^{n'} c^{\text{o}}_{\text{ML}_s^{z+}} + c^{\text{o}}_{\text{H}^+} = c^{\text{o}}_{\text{Y}^-} + c^{\text{o}}_{\text{X}^-} + c^{\text{o}}_{\text{HO}^-} \tag{A8}$$

where c_i^{α}, is the concentration of the *i*-species in the α-phase (α = w or o).

According to the Nernst equation, the concentration ratio, $c_i^{\text{o}}/c_i^{\text{w}}$, can be expressed as:

$$\frac{c_i^{\text{o}}}{c_i^{\text{w}}} = \left(\frac{\gamma_i^{\text{w}}}{\gamma_i^{\text{o}}}\right)(\theta_{\text{eq}}\theta_i)^{z_i} \tag{A9}$$

where z_i is the charge of the *i*-species, $\theta_{eq} = \exp\left(\frac{F}{RT}\Delta^{\text{w}}_{\text{o}}\phi_{\text{eq}}\right)$, $\theta_i = \exp\left(-\frac{F}{RT}\Delta^{\text{w}}_{\text{o}}\phi^{\text{o}}_i\right)$, $\Delta^{\text{w}}_{\text{o}}\phi_{\text{eq}}$ is the distribution potential and $\Delta^{\text{w}}_{\text{o}}\phi^{\text{o}}_i$ is the standard transfer potential of the *i*-species. Although the activity coefficients, γ_i^{α}, are functions of the composition of the solution phase, we neglect the concentration dependence of the activity coefficients for simplicity reasons.

Water autoprotolysis is explicitly considered as [38]:

$$H_2O \rightleftarrows H^+ + HO^-$$

The water autoprotolysis constant is defined by:

$$K_{\text{w}} = c^{\text{w}}_{\text{H}^+}c^{\text{w}}_{\text{HO}^-} \tag{A10}$$

and the 1:*s* complex formation constants, $K^{\alpha}_{\text{ML}_s^{z+}}$, are defined by Eq. (1) in the present work.

Eqs. (A1)–(A8) may be solved numerically using the Powell hybrid method [44–46] according with the methodology developed in Ref. [38].

References

[1] Z. Samec, Pure Appl. Chem. 76 (2004) 2147–2180.
[2] R.A. Iglesias, S.A. Dassie, Ion Transfer at Liquid/Liquid Interfaces, Nova Publishers, New York, 2010.
[3] J. Koryta, P. Vanýsek, M. Březina, J. Electroanal. Chem. 67 (1976) 263–266.
[4] S. Kihara, M. Suzuki, K. Maeda, K. Ogura, M. Matsui, J. Electroanal. Chem. 210 (1986) 147–159.
[5] S. Wilke, H. Franzke, H. Müller, Anal. Chim. Acta 268 (1992) 285–292.
[6] S. Wilke, Anal. Chim. Acta 295 (1994) 165–172.
[7] B. Hundhammer, T. Solomon, T. Zerihun, M. Abegaz, A. Bekele, K. Graichen, J. Electroanal. Chem. 371 (1994) 1–11.
[8] V. Mareček, H. Jänchenová, M.P. Colombini, P. Papoff, J. Electroanal. Chem. 217 (1987) 213–219.
[9] P. Liljeroth, C. Johans, K. Kontturi, J.A. Manzanares, J. Electroanal. Chem. 483 (2000) 37–46.
[10] S.S. Hill, R.A.W. Dryfe, E.P.L. Roberts, A.C. Fisher, K. Yunus, Anal. Chem. 75 (2003) 486–493.
[11] F.G.E. Jones, R.A.W. Dryfe, J. Electroanal. Chem. 615 (2008) 25–33.
[12] W.J. Albery, A.M. Couper, J. Hadgraft, C. Ryan, J. Chem. Soc. Faraday Trans. 70 (1974) 1124–1131.
[13] J. Albery, J.F. Burke, E.B. Leffler, J. Hadgraft, J. Chem. Soc. Faraday Trans. 72 (1976) 1618–1626.
[14] W.J. Albery, R.A. Choudhery, J. Phys. Chem. 92 (1988) 1142–1151.
[15] J.A. Manzanares, R. Lahtinen, B. Quinn, K. Kontturi, D.J. Schiffrin, Electrochim. Acta 44 (1998) 59–71.
[16] B. Kralj, R.A.W. Dryfe, J. Phys. Chem. B 106 (2002) 6732–6739.
[17] B. Kralj, R.A.W. Dryfe, J. Electroanal. Chem. 560 (2003) 127–133.
[18] K. Fujii, S. Tanibuchi, S. Kihara, Anal. Sci. 21 (2005) 1415–1420.
[19] G. Taylor, H.H. Girault, J. Electroanal. Chem. 208 (1986) 179–183.
[20] Y. Ohkouchi, T. Kakutani, T. Osakai, M. Senda, Anal. Sci. 7 (1991) 371–376.
[21] J.A. Campbell, H.H. Girault, J. Electroanal. Chem. 266 (1989) 465–469.
[22] A.A. Stewart, G. Taylor, H.H. Girault, J. McAleer, J. Electroanal. Chem. 296 (1990) 491–515.
[23] A.A. Stewart, Y. Shao, C.M. Pereira, H.H. Girault, J. Electroanal. Chem. 305 (1991) 135–139.
[24] N. Wilke, R.A. Iglesias, S.G. Chesniuk, S.A. Dassie, A.M. Baruzzi, Bull. Chem. Soc. Jpn. 75 (2002) 235–240.
[25] M.A. Fernández, L.M. Yudi, A.M. Baruzzi, Electroanalysis 16 (2004) 491–496.
[26] R.A. Fernández, S.A. Dassie, J. Electroanal. Chem. 624 (2008) 121–128.
[27] R.A. Fernández, M.I. Velasco, L.I. Rossi, S.A. Dassie, J. Electroanal. Chem. 650 (2010) 47–54.
[28] R.S. Nicholson, I. Shain, Anal. Chem. 36 (1964) 706–723.
[29] V.G. Levich, Physicochemical Hydrodynamics, Prentice-Hall, Englewood Cliffs, NJ, 1962.
[30] M.C. Ribeiro, L.G.C. Rego, P.C.T. D'Ajello, J. Electroanal. Chem. 628 (2009) 21–26.
[31] V.S. Bagotsky, Fundamentals of Electrochemistry, John Wiley & Sons, New Jersey, 2008.
[32] J.I. Garcia, R.A. Fernández, A.J. Ruggeri, S.A. Dassie, J. Electroanal. Chem. 594 (2006) 80–88.
[33] J.I. Garcia, R.A. Iglesias, S.A. Dassie, J. Electroanal. Chem. 586 (2006) 225–236.
[34] J.I. Garcia, M.B. Oviedo, S.A. Dassie, J. Electroanal. Chem. 645 (2010) 1–9.
[35] L.Q. Hung, J. Electroanal. Chem. 115 (1980) 159–174.
[36] L.Q. Hung, J. Electroanal. Chem. 149 (1983) 1–14.
[37] T. Kakiuchi, Anal. Chem. 68 (1996) 3658–3664.
[38] J.I. Garcia, R.A. Fernández, S.A. Dassie, T. Kakiuchi, J. Electroanal. Chem. 640 (2010) 42–50.
[39] D.K. Gosser, Cyclic Coltammetry: Simulation and Analysis of Reaction Mechanisms, VCH Publishers, New York, 1993.
[40] J.T. Malloy, in: W.R. Kissinger, P.T. Heinman (Eds.), Laboratory Techniques in Electroanalytical Chemistry, second ed., Marcel Dekker, New York, 1996, pp. 583–621.
[41] P.T. Kissinger, C.R. Preddy, R.E. Shoup, W.R. Hieneman, in: P. Kissinger, W. Heineman (Eds.), Fundamentals Concepts of Analytical Electrochemistry in Laboratory Techniques in Electroanalytical Chemistry, second ed., Marcel Dekker, New York, 1996, pp. 11–50.
[42] A.J. Bard, C.R. Faulkner, Electrochemical Methods Fundamentals and Applications, second ed., John Wiley & Sons, New York, 2001.
[43] D. Britz, Digital Simulation in Electrochemistry, third ed., Springer, Berlin, Heidelberg, 2005.
[44] W.H. Press, S.A. Teukolsky, I.T. Vetterling, B.P. Flannery, Numerical Recipes in Fortran 77: The Art of Scientific Computing, second ed., Cambridge University Press, 1992.
[45] R.L. Burden, J.D. Douglas Faires, Análisis Numérico, Grupo Editorial Iberoamérica, México, 1985.
[46] Subroutines in Fortran, 2011. <http://www.netlib.org>.
[47] M.D. Osborne, H.H. Girault, Electroanalysis 7 (1995) 425–434.
[48] Y. Shao, M.D. Osborne, H.H. Girault, J. Electroanal. Chem. 318 (1991) 101–109.
[49] F. Reymond, P.-A. Carrupt, H.H. Girault, J. Electroanal. Chem. 449 (1998) 49–65.